Title	Full-range and long-term behaviour of prestressed concrete bridges with corrugated steel webs
Author(s)	Au, FTK; CHEN, X; Jiang, R; Huang, T
Citation	Journal of Civil Engineering Research, 2017, v. 7 n. 2, p. 35-45
Issued Date	2017
URL	http://hdl.handle.net/10722/247320
Rights	This work is licensed under a Creative Commons Attribution-NonCommercial-NoDerivatives 4.0 International License.

Journal of Civil Engineering Research 2017, 7(2): 35-45
DOI: 10.5923/j.jce.20170702.01

Full-range and Long-term Behaviour of Prestressed Concrete Bridges with Corrugated Steel Webs

Francis T. K. Au[1,*], X. C. Chen[1,2], R. J. Jiang[3], T. Huang[1]

[1]Department of Civil Engineering, The University of Hong Kong, Hong Kong, China
[2]Research and Technology Center, WISE-TECH Engineering Consulting Co. Ltd, Shenzhen, China
[3]Research Center, Shenzhen Municipal Engineering Design and Research Institute, Shenzhen, China

Abstract Prestressed concrete bridges with corrugated steel webs have emerged as a promising bridge form due to their remarkable advantages such as efficient prestressing of concrete, high buckling strength of steel webs and lightness. The full-range and long-term behaviour of these bridges was studied both numerically and experimentally. A sandwich beam theory was developed to investigate both the static and dynamic behaviour numerically. In the development of numerical models, special emphasis was placed on the modelling of corrugated steel webs, external prestressing tendons, diaphragms, and the interaction between web shear deformation and local flange bending. The numerical models were verified by tests. By using the numerical models proposed, the static service behaviour, dynamic properties and long-term behaviour were studied. The sectional ductility, deformability and strength were evaluated by nonlinear analysis taking into account the actual stress-strain curves and path-dependence of materials. The failure mechanisms were studied experimentally and numerically for more accurate evaluation of safety-related attributes such as ultimate load, ductility and deformability. The formation of plastic hinge and its size were also studied thoroughly in view of their importance in the prediction of full-range behaviour. The long-term behaviour was also studied numerically and experimentally. Some design recommendations are provided here.

Keywords Corrugated steel webs, Full-range behaviour, Long-term behaviour, Prestressed concrete

1. Introduction

In the search for efficient structural forms for bridges, prestressed concrete bridges with corrugated steel webs as shown in Figure 1 have emerged as a promising solution. This form of bridge has some remarkable advantages such as lightness, high buckling strength of steel webs, efficient prestressing of concrete, and easy maintenance. In 1986, the first bridge of this type, Cognac Bridge, was built in France [1]. Its successful application and various advantages over the conventional prestressed concrete bridges have prompted researchers and construction companies in various countries, including Japan, USA, China, Germany, etc. to continue with the relevant work in research and development. Over 200 concrete bridges with corrugated steel webs have been built. Hereafter in this paper, this form of bridge is assumed unless otherwise stated.

Despite various merits brought along by the corrugated steel webs, there are also some concerns in this type of bridges. The prestressed concrete bridges with corrugated steel webs are known to be less stiff than those with conventional concrete webs, which leads to larger deflections. Even though some initial design guidance has been formulated, *e.g.* Research Group of Composite Structure with Corrugated Steel Web [2], there are still various issues to resolve. Owing to large shear deformation and negligible axial stiffness of corrugated steel webs, the assumption that plane sections remain plane may not be valid, and therefore the conventional Euler-Bernoulli and Timoshenko beam theories cannot be applied to this form of bridges [3]. Besides, the application of external prestressing in addition to internal prestressing in these bridges implies that their structural behaviour is governed not only by individual sections but also by the overall global behaviour of the structural system due to the unbonded nature of external prestressing tendons. As the problem is obviously different from conventional prestressed concrete bridges with external prestressing tendons in view of the high flexibility of corrugated steel webs, further in-depth study is desirable. Practical yet reliable models for analyses of concrete bridges with corrugated steel webs and external tendons are needed to accurately predict their static, dynamic and long-term behaviour.

The full-range behaviour of the bridges covering both the service and failure stages is rather complicated due to the material and geometric nonlinearities, possible buckling of corrugated steel webs, interaction among components of different properties, presence of external prestressing tendons, etc., which should be systematically studied. The

* Corresponding author:
francis.au@hku.hk (Francis T. K. Au)
Published online at http://journal.sapub.org/jce

prediction of full-range behaviour is required in the evaluation of various safety-related attributes, *e.g.* ultimate load, ductility and deformability. Moreover, this bridge form has tactfully utilised the strength and lightness of high-strength concrete, and the brittleness of high-strength concrete may raise the concern of possible progressive failure caused by premature rupture of brittle concrete flanges. Reliable methods for full-range analysis will assure not only robustness of structural behaviour but also realistic estimation of internal force redistribution at inelastic stages. To obtain the post-elastic branch of structural response, it is necessary to take into account geometric nonlinearity as well as material nonlinearity and stress-path dependence.

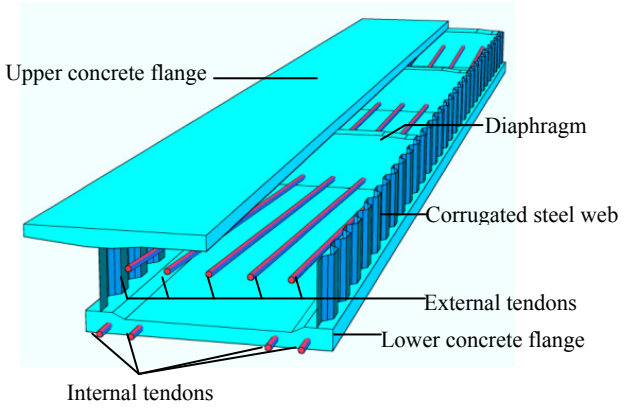

Figure 1. A prestressed concrete bridge with corrugated steel webs (some parts of the bridge are omitted for clarity)

In this study, the main objectives are:

(a) To develop unified models for service behaviour, including not only static and dynamic responses, but also long-term behaviour taking into account concrete creep and shrinkage, and prestressing steel relaxation;
(b) To study the sectional ductility, deformability and strength of the reinforced and prestressed concrete sections with corrugated steel webs;
(c) To study the nonlinear structural behaviour of the bridge in the presence of external tendons;
(d) To study the failure mechanisms under loading for more accurate evaluation of safety-related attributes such as ultimate load, ductility and deformability; and
(e) To formulate rational design guidance for this kind of bridges.

This study involves both experimental and numerical investigations. The results of experimental work are used to calibrate and to guide the formulation of numerical models. A comprehensive parametric study was carried out to investigate the effects of various parameters such as section properties, material properties, reinforcement ratio, prestressing level, arrangement of external tendons, etc.

2. Experimental Programme

This section illustrates the experimental programme, while the verification and calibration of the proposed numerical models using the experimental results are described in the subsequent sections.

2.1. Experimental Programme for Static and Dynamic Behaviour

Some prestressed concrete beam specimens with corrugated steel web were fabricated for testing. One sample is shown in Figure 2. The flanges of these specimens were cast of high-strength concrete. The thickness of corrugated steel webs was 5 mm. Embedment connections were provided between the concrete flanges and corrugated steel web.

Figure 2. One of the tested beams

The specimens tested are summarised in Table 1. Specimens A-1, A-2, P-1, B-1, B-2, B-3 and B-4 were fabricated for both dynamic and static tests. Shortly after post-tensioning and before mounting the setup for static loading tests, each specimen was tested for its dynamic properties using an instrumented hammer and accelerometers mounted along the beam. After the dynamic measurements, static loading tests were carried out.

Load cells were used at the end of each tendon to monitor the variation of tendon force during tensioning and the subsequent loading test. Linear variable differential transformers (LVDTs) were used to measure displacements during the test. Strain gauges were provided on concrete surface and steel bars at selected sections for monitoring of normal strains. Strain gauge rosettes were provided at selected points of the web surface for monitoring of shear strains.

In the tests, the following aspects were studied in detail:

(a) Dynamic responses (natural frequencies and mode shapes) and initial static responses for calibration of models for service behaviour;
(b) Load-displacement relation, variation of tendon forces, etc. for full-range behaviour;
(c) Failure mechanism; and
(d) Formation and size of plastic hinges.

2.2. Experimental Programme for Long-term Time-dependent Behaviour

A prestressed concrete beam with a single corrugated steel web, namely Specimen L-1 as shown in Table 1, was fabricated for long-term monitoring. The specimen, cast of grade C60 concrete, was simply supported and

post-tensioned by an initial effective prestressing force of 200.95 kN. Three dial gauges were used to measure the variations of deflection with time, while the variations of prestress were measured by load cells under the anchorages.

Table 1. Summary of Tested Specimens

Specimen No.	Span (mm)	Beam depth (mm)	Flange thickness (mm)	Diaphragm thickness (mm)		Tendon type	No. of deviators	Loading scheme (displacement control)
				End	Intermediate			
A-1	4500	300	50	200	70	Two external SS*	2	Monotonic third-point loading
A-2	2×2250	300	50	200	200 or 70	Two external SS*	3	Monotonic point loading at each mid-span
P-1	4500	300	50	200	70	Two internal bonded SS*	2	Monotonic third-point loading
B-1	3600	360	80	200	-	Two external SS*	0	Non-reversed cyclic loading
B-2	3600	360	80	200	70	Two external SS*	1	Non-reversed cyclic loading
B-3	3600	360	80	200	-	-	0	Non-reversed cyclic loading
B-4	3600	360	80	200	70	Two external AFRP-R^	1	Non-reversed cyclic loading
L-1	2800	300	50	160	-	Two external SS*	0	-

Notes: *SS stands for 7-wire steel strand with a diameter of 12.7 mm and a cross-sectional area of 98.7 mm^2;
^AFRP-R strands for aramid fibre reinforced polymer rope with a cross-sectional area of 54.5 mm^2.

3. An Extended Sandwich Beam Model

3.1. Beam Model

Corrugated steel sheets can be analysed by the theory of orthotropic plates [4]. Elgaaly *et al*. [5], Combault [6], and Johnson and Cafolla [7] found the axial stiffness of corrugated steel web negligible.

The sandwich beam model proposed by Chen *et al.* [8] and Chen *et al.* [9] for this type of bridges is adopted. Figure 3(a) shows the simplified typical cross section characterised by the height h_w of web and the distance h between centroidal axes of flanges, and Figure 3(b) shows the typical corrugations. The corrugated steel sheet is modelled as an orthotropic plate.

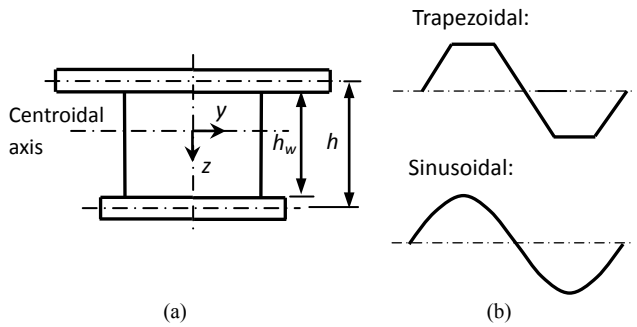

Figure 3. Configuration of bridge: (a) A simplified cross section; and (b) One full corrugation of steel web

After taking into account the interaction between bending deflection v_1 and shear deflection v_2, which may cause additional local curvature of the flanges due to discontinuous shear force [8], the governing equation is obtained as

$$\left[-B\frac{\partial^4 v}{\partial x^4}+q\right]+\left[\frac{B}{\alpha^2 B_f}\left(-\frac{\partial^2 q}{\partial x^2}\right)\right]+\left[\frac{B}{\alpha^2}\frac{\partial^6 v}{\partial x^6}\right]=0 \qquad (1)$$

where $v=v_1+v_2$ and $B = B_g+B_f$ with B_f being the sum of local flexural rigidities of flanges about their respective centroidal axes and B_g being the global flexural rigidity of flanges about the centroidal axis of the entire beam section assuming uniform stress in each flange; $\alpha^2=\left(\beta^2 S_w/B_f\right)\left(B/B_g\right)$ with S_w being the shear rigidity of corrugated webs; $\beta = h/h_w$; and q is the distributed load.

The terms within the first set of square brackets represent the basic case without shear deformation, *i.e.* the case of Euler-Bernoulli beam. The term in the second set of square brackets arises from web shear deformation. The term in the third set of square brackets results from the interaction between web shear deformation and local bending of flanges.

A C^1 three-node beam finite element is formulated with its displacement vector comprising the longitudinal displacement u of the beam axis, deflection v and normal rotation φ, which are interpolated by linear, Hermite cubic and quadratic polynomials respectively. With the nodes labelled locally as a, b and c from the left end of element, the element displacement vector is $\left\{u_a \;\; v_a \;\; v'_a \;\; \varphi_a \;\; \varphi_b \;\; u_c \;\; v_c \;\; v'_c \;\; \varphi_c\right\}^{\mathrm{T}}$. As the constraint index count of the shear stiffness matrix is above zero, there is low risk of shear locking.

3.2. Diaphragms

These bridges are often provided with end and intermediate diaphragms. The diaphragm resists the adjacent web shear deformation and prevents the relative longitudinal movement of the flanges.

The action of the k-th diaphragm located at an edge node of element can be modelled by an internal couple, which needs to satisfy the condition of compatibility and equilibrium at the web-flange junction at the diaphragm [8], resulting in the strain energy $U_{dia,k}$ as

$$U_{dia,k} = \frac{1}{2}(\mathbf{d}_k)^{\mathrm{T}} \mathbf{k}_{dia,k} \mathbf{d}_k \quad (2)$$

where $\mathbf{d}_k$ is the displacement vector at the node; and the additional stiffness matrix $\mathbf{k}_{dia,k}$ caused by the diaphragm is given by

$$\mathbf{k}_{dia,k} = K_d h^2 \begin{bmatrix} 0 & 0 & 1 & 1 \end{bmatrix}^{\mathrm{T}} \begin{bmatrix} 0 & 0 & 1 & 1 \end{bmatrix} \quad (3)$$

where K_d is the equivalent stiffness of the diaphragm associated with the relative longitudinal movement.

3.3. External Tendons

The external tendons interact with the beam through anchorages and deviators. The elongation of external tendons depends on the global bridge deformation. The model of Dall'Asta *et al.* [10] for externally prestressed Euler-Bernoulli beams has been extended by Chen *et al.* [9] for this type of bridges.

In brief, the profile of the external tendon is defined by the positions of end anchorages or intermediate deviators, and the additional elongation and strain of the tendon are calculated from the initial and deformed total lengths accordingly. The mesh is so chosen that the (n+1) deviators or anchorages coincide with some of the k end nodes of elements. The strain of external tendon is then obtained from the beam displacements as

$$\varepsilon_p = \frac{1}{L_{t0}} \boldsymbol{\chi} \mathbf{D} \quad (4)$$

where $\mathbf{D}$ is the global nodal displacement vector of the beam; and $\boldsymbol{\chi}$ is the kinematic compatibility matrix to extract the necessary displacements from the global displacement vector.

The strain energy U_{p} in the external tendon is

$$U_p = \frac{1}{2} L_{t0} A_p \sigma_p \varepsilon_p = \frac{1}{2} \mathbf{D}^{\mathrm{T}} \mathbf{K}_p \mathbf{D} \quad (5)$$

where L_{t0}, A_p, σ_p and E_p are the initial total length, cross-sectional area, stress and modulus of elasticity of the tendon respectively; and $\mathbf{K}_p$ is the associated stiffness given by

$$\mathbf{K}_p = \frac{E_p A_p}{L_{t0}} \boldsymbol{\chi}^{\mathrm{T}} \boldsymbol{\chi} \quad (6)$$

The equivalent load vector resulting from stressing the external tendon is $\mathbf{F}_p = A_p \sigma_p \boldsymbol{\chi}$.

The external tendons and beam with diaphragms work together as a structural system. Applying the principle of minimum total potential energy then yields the necessary equation.

4. Flexural Ductility of Reinforced and Prestressed Concrete Sections

In the design of concrete bridges with corrugated steel webs, especially those with flanges made of high-strength concrete and/or those with the requirement of seismic resistance, the flexural ductility and deformability as well as strength need to be carefully examined. Evaluation of these safety-related attributes requires the reliable estimation of full-range behaviour that encompasses the service and failure behaviour.

4.1. Method of Analysis

In this study, the moment-curvature relation of reinforced concrete and partially prestressed concrete sections with corrugated steel webs is evaluated by means of a nonlinear numerical method which uses the actual stress-strain curves of the materials and considers their stress-path dependence [11, 12]. The properties of ordinary non-prestressed reinforcement and prestressing steel are also incorporated in the method so that both reinforced concrete and partially prestressed concrete sections can be studied. The material laws considering strain reversal are adopted. Figure 4(a) shows the model for both unconfined and confined concrete comprising the stress-strain curve in compression developed by Attard and Setunge [13] and that in tension proposed by Carreira and Chu [14], and Guo and Zhang [15]. The stress-strain curve recommended by Mander et al. [16] is used for non-prestressed steel as shown in Figure 4(b). The stress-strain formula for prestressing steel proposed by Menegotto and Pinto [17] is adopted here as shown in Figure 4(c). The AFRP rope is linearly elastic up to failure and has no significant yielding.

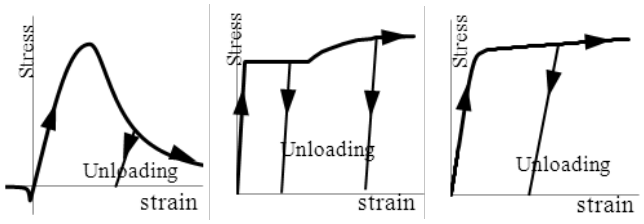

Figure 4. Stress-strain curves of materials: (a) concrete; (b) non-prestressed steel; and (c) prestressing steel

For a section with negligible interaction effects, in each iteration cycle, the strain variation is determined assuming linear strain distribution over the section depth according to the prescribed curvature ϕ as shown in Figure 5(a), and the stresses in the concrete and steel components are evaluated from their respective constitutive models accordingly. When the interaction effects need to be considered especially in the vicinity of a point load or diaphragm, in addition to the primary curvature ϕ_1 that is based on the average axial strain of each of the concrete flanges, the secondary local curvature ϕ_2 in concrete flanges as shown in Figure 5(b) should be considered. An iterative process is adopted such that the primary curvature ϕ_1 is prescribed incrementally and the secondary local curvature ϕ_2 is determined accordingly from sectional and structural equilibrium. The total curvature ϕ is the sum of the primary curvature ϕ_1 and the local

secondary curvature ϕ_2, *i.e.* $\phi = \phi_1 + \phi_2$. Axial equilibrium is used to determine the neutral axis depth d_n, after which the resisting moment is calculated. This iterative process is repeated until sufficient length of the full-range moment-curvature curve has been obtained.

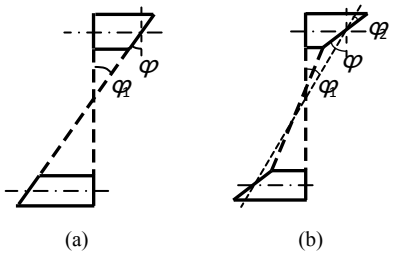

Figure 5. Strain distribution over section depth: (a) Without interaction effects ($\phi_2 = 0$); and (b) With interaction effects ($\phi_2 \neq 0$)

The numerical model developed has been verified by experiments on Specimen P-1 [18]. An extensive parametric study has also been conducted to examine the effects of various parameters, such as the section shape, grade of concrete, steel content, partial prestressing ratio, prestressing force ratio, *etc.*, on the ductility, deformability and strength of the bridge section [18].

4.2. Effects of Interaction between Web Shear Deformation and Local Bending of Flanges

To consider the interaction effects in the section analysis, the secondary curvature ϕ_2 associated with additional local bending induced in the concrete flanges is determined upon application of the primary curvature ϕ_1 to the entire section. The values of α and B_f are updated accordingly to account for material nonlinearity as necessary.

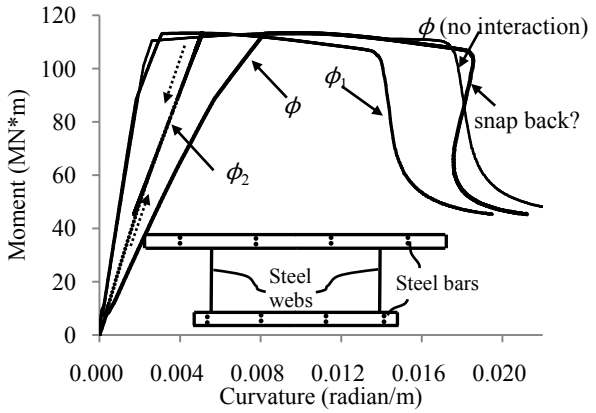

Figure 6. Complete moment-curvature curves considering interaction effects

The complete moment-curvature curve of the mid-span section of a simply-supported beam with corrugated webs considering interaction effects are obtained and compared with that ignoring interaction effects as shown in Figure 6. It shows that interaction has little effect on the ultimate curvature and deformability, but significantly increases the yield curvature and reduces the ductility. The total curvature ϕ considering interaction effects is found to reverse when the resisting moment M drops significantly, giving rise to a "snap back" phenomenon. It is because the secondary curvature ϕ_2 decreases with the drop of resisting shear force V and bending moment M. This should be treated with caution, as the upper concrete flange may be crushed, thereby creating a kink and violating the assumptions made in the numerical model. Nevertheless, the effects of the curvature reversal on the sectional strength, ductility and deformability are insignificant.

The "snap back" phenomenon is observed in the test results of B-4 as shown in Figure 7.

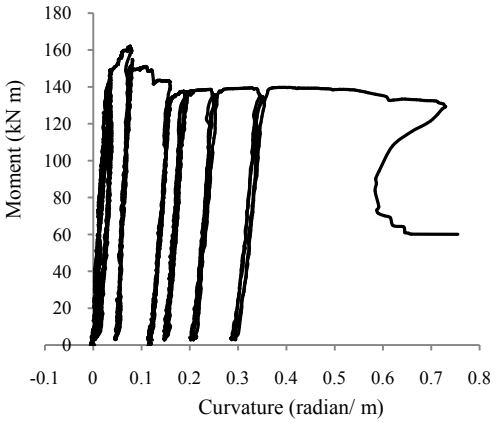

Figure 7. Moment-curvature curve for mid-span section of Specimen B-4

The interaction effects are found to be sensitive to the span L and the parameter α. As the span L decreases, the yield curvature increases. With the reduction of the parameter α, the yield curvature increases too.

5. Formation of Plastic Hinges

It is inspiring to study the formation of plastic hinges in these bridges and their effect on the full-range behaviour that covers both the pre-peak-strength and post-peak- strength structural responses. The presence of shear-deformable corrugated steel webs with negligible axial stiffness and prestressing tendons certainly complicates the formation of plastic hinges. Hence in this study, the critical region length, performance of the plastic hinge and full-range behaviour of the bridges are studied.

5.1. Flexural Failure Mode

It is observed in the tests that tensile cracks appeared first in the lower flange in the potential plastic zone around the mid-span. With the increase in loading, the tensile steel yielded and the neutral axis shifted towards the upper flange, placing the bottom of the upper flange in tensile zone. The secondary moment caused further tension and led to cracking at the bottom of the upper flange. As the displacement further increased, tensile cracks in the upper flange gradually extended upwards, followed by the crushing of top concrete. Shear crack also occurred in the upper flange later. To

illustrate, the plastic hinges formed in Specimens B-1 and B-4 are shown in Figures 8(a) and 8(b) respectively.

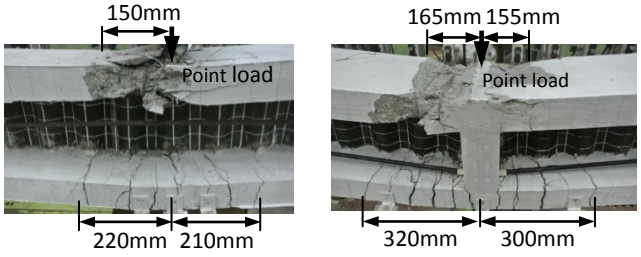

Figure 8. Plastic hinge zones and critical region lengths: (a) Specimen B-1; and (b) Specimen B-4

It should be noted that two types of hinging have actually developed, *i.e.* "full-depth plastic hinge" and "flange plastic hinge". In addition to the "full-depth plastic hinge", which was related to global structural behaviour, the interaction between the shear deformation of corrugated steel webs and local bending of concrete flanges caused formation of local plastic hinge in the upper flange. It is referred to as the "flange plastic hinge" here. It is essential to understand the interaction between the flange plastic hinge and full-depth plastic hinge.

5.2. Critical Region Lengths and Plastic Hinge Lengths

As the critical region length in the upper flange is closely related to the formation of flange plastic hinge, which is similar to a column plastic hinge, the critical region length in the upper flange is taken to include regions having [19]: (a) spalling of concrete cover; (b) penetration of spalling into concrete core region; (c) local buckling of longitudinal steel; and (d) tensile cracks at flange bottom by visual inspection. On the other hand, the critical region length in the lower flange is closely related to the full-depth plastic hinge and hence includes the region which suffers from significant tensile cracking [19]. After finishing the tests, all the loose concrete pieces were removed to expose the degree of damage before taking photographs. The observed critical regions of specimens are illustrated in Figure 8, together with the estimated critical region lengths. The plastic hinge in the upper flange is relatively small as compared to the full-depth plastic hinge length.

The interaction between the critical region lengths in the upper and lower flanges results in an "interactive critical region length" l_c. It is approximated as the length of the region between the sections that has sustained a rotation equal to the yield slope θ_y. This is illustrated in Figure 9. Transverse reinforcement should be provided within the critical region for effective confinement and strengthening of concrete.

Similarly, due to the interaction between the flange and full-depth plastic hinges, the so-called "equivalent interactive plastic hinge length" l_p is devised. In contrast to conventional beams and columns, the curvature at the free end of the present specimen was not zero but substantially reversed because of the diaphragm effect. Hence, the "equivalent interactive plastic hinge length" may be solved from

$$\theta_{end} = (1/2)\phi_y (L/2) + (\phi_u - \phi_y) l_p - \phi_{2,dia\_p} (1/\alpha) \qquad (7)$$

where θ_{end} is the specimen-end slope at ultimate; ϕ_u is the ultimate curvature at the critical section; ϕ_{2,dia_p} is the peak secondary curvature around the end diaphragm, and the third term on the right-hand side is the integral of secondary curvature around the end diaphragm along the span.

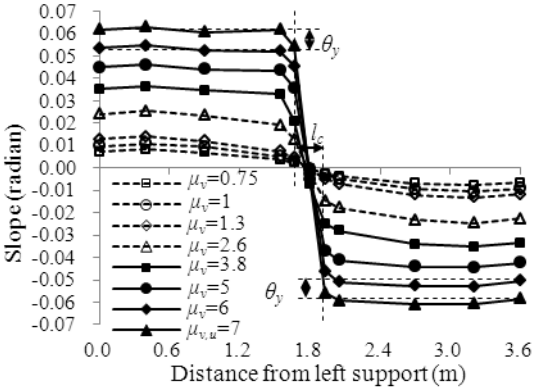

Notes:
μ_v denotes ductility factor for mid-span deflection;
$\mu_{v,u}$ denotes deflection ductility factor at ultimate.

Figure 9. Specimen B-1: Measured slope

Table 2 shows that while the interactive critical region length l_c of Specimen B-4 is around twice that of Specimens B-1 to B-3 due to that the flange plastic hinge fully formed on both sides of mid-span instead of only one side, the equivalent interactive plastic hinge length of Specimen B-4 is also twice that of Specimens B-1 to B-3. One may conclude that the flange plastic hinge governs the equivalent interactive plastic hinge length and that the plastic behaviour will mainly rely on the performance of the plastic hinge in the upper flange.

Table 2. Measured Critical Region Length, Interactive Critical Region Length and Equivalent Plastic Hinge Length

Specimen	Critical region length (mm)						Interactive plastic hinge length (mm)	
	Upper flange		Lower flange		Interactive			
	Left side	Right side	Left side	Right side	(Total)			
B-1	150	-	220	210	238	$3.3t_u$	123	$1.5t_u$
B-2	160	-	290	105	310		130	
B-3	-	155	305	305	235		116	
B-4*	165	155	320	300	490	$6.1t_u$	219	$2.7t_u$

* Upper flange plastic hinge formed on both sides of critical section;
t_u is the thickness of upper flange.

The relation between the various plastic hinge lengths and critical region lengths is summarised in Figure 10.

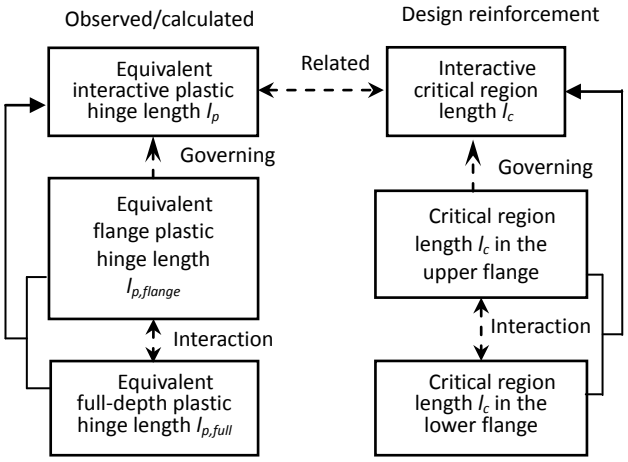

Figure 10. Relation between various plastic hinge lengths and critical region lengths

5.3. Interaction between Flange Plastic Hinges and Full-depth Plastic Hinge

As elaborated in Section 5.2, the flange plastic hinge governs the full-range structural behaviour of the bridge, indicating that the equivalent interactive plastic hinge length l_p is close to the equivalent flange plastic hinge length, while the effects of full-depth plastic hinge should also be taken into account. A simple formula for prediction of the equivalent interactive plastic hinge length l_p was proposed as [20]

$$l_p = l_{p,\,flange} + 0.2 l_{p,\,full} \tag{8}$$

where $l_{p,\,flange}$ is the equivalent flange plastic hinge length in accordance with Sheikh and Khoury [21], Bayrak and Sheikh [22] or Subramanian [23]; and $l_{p,\,full}$ is the equivalent full-depth plastic hinge length in accordance with Baker [24]. The coefficient 0.2 has been obtained by linear regression analysis of results.

5.4. Simplified Method for Prediction of Full-Range Structural Behaviour

When the plastic hinge length and sectional moment-curvature curves of a bridge are known, the deflection and slope can be obtained by integration of curvature along the span. Here, the full-range structural behaviour of this type of bridge is predicted based on the concept of the equivalent plastic hinge length. The second-order effects associated with the external tendons are also considered. For rigorous procedure, one may refer to Chen *et al*. [25]. In the proposed simplified method, the load-displacement and load-tendon-stress curves are approximated by tri-linear relationship as shown in Figure 11, where P_{yield} and P_{peak} are the yielding and ultimate load respectively. It then reduces to analyse the structural states with the critical section having the yield, peak and ultimate curvature in turn, which are determined from the moment-curvature analysis first.

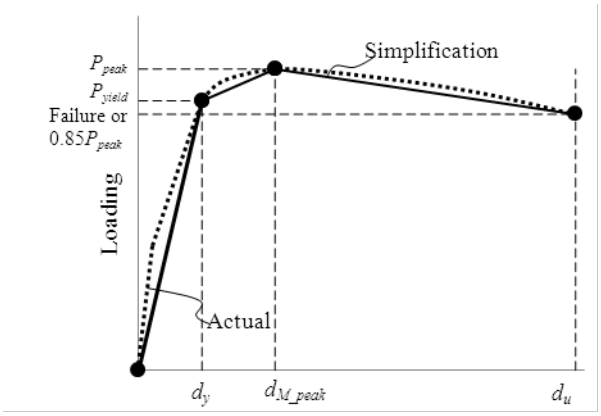

Figure 11. Actual and simplified load-displacement curves

Using the simplified method, the relations between the load and mid-span deflection and tendon stress for Specimens B-1 are predicted and compared with the measured hysteresis envelopes as shown in Figure 12, which show reasonably good agreement.

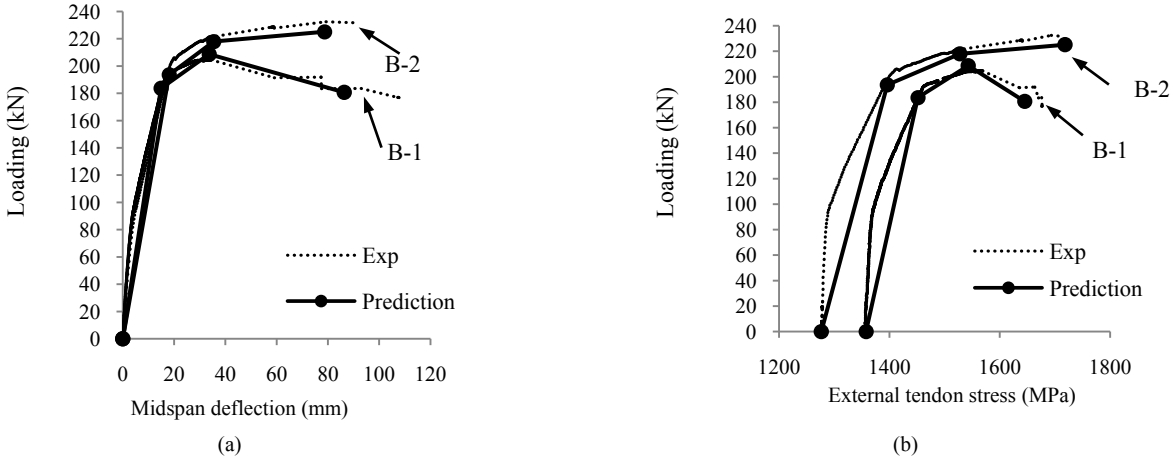

Figure 12. Full range structural behaviour of Specimens B-1 and B-2: (a) load vs. mid-span deflection; (b) load vs. tendon stress

6. Dynamic Properties

Prestressed concrete bridges with corrugated steel webs are especially popular in regions of strong seismicity since they are lighter than conventional prestressed concrete bridges. However, the reduction in self-weight is also accompanied by reduction in stiffness [26]. Moreover, external prestressing tendons are usually adopted along with internal tendons, and diaphragms are always provided not only to act as deviators but also to improve the torsional resistance. All these may affect the dynamic properties.

The sandwich beam model described in Section 3, which takes into account the presence of the diaphragms, the external prestressing tendons and the interaction between the web shear deformation and the flange local bending, was employed to predict the vibration characteristics of this type of bridges. The governing equation of free vibration can be obtained as

$$\left[-B\frac{\partial^4 v}{\partial x^4}-m\ddot{v}+q\right]+\left[\frac{B}{\alpha^2 B_f}\left(m\frac{\partial^2 \ddot{v}}{\partial x^2}-\frac{\partial^2 q}{\partial x^2}\right)\right]+\left[\frac{B}{\alpha^2}\frac{\partial^6 v}{\partial x^6}\right]=0 \quad (9)$$

To further understand the dynamic behaviour of this type of bridges, the classical Euler-Bernoulli and Timoshenko beam models were also evaluated [9]. Dynamic tests were carried out as described in Section 2. As an example, the test results of the first three natural frequencies of Specimens A-1 are compared with the numerical results as shown in Table 3.

Table 3. Experimental and Numerical Results of First Three Natural Frequencies of Specimen A-1

	Frequencies (Hz)		
	1st Mode	2nd Mode	3rd Mode
Experimental	32.221	116.546	250.529
	Deviation from experimental result		
Sandwich beam (with external tendons)	-0.51%	0.25%	0.45%
Sandwich beam (without external tendons)	-0.08%	1.20%	0.45%
Euler-Bernoulli beam (with external tendons)	2.73%	12.95%	25.40%
Timoshenko beam (with external tendons)	-1.50%	-3.05%	-6.28%

The frequencies calculated by the sandwich beam theory agree well with the experimental results, while results from Euler-Bernoulli beam and Timoshenko beam models are higher and lower than the experimental results, respectively. It suggests that the sandwich beam model can accurately predict the dynamic properties of this type of bridge. It is also found that the sandwich beam model performs better than the classic beam models especially for bridges with short spans and/or lower ratios of section shear rigidity to flange local bending rigidity.

7. Long-term Time-dependent Behaviour

Although many researchers have studied their structural behaviour, relatively little effort has been devoted to their long-term behaviour [25]. The long-term effects may result in additional deflections, loss of prestress, force redistribution and possibly additional cracking.

The long-term structural behaviour is analysed using the nonlinear numerical method developed in conjunction with time-dependent material properties. Specifically, the Eurocode models for concrete creep and tendon relaxation were adopted. As the granitic aggregate available around Hong Kong has relatively low elastic modulus and high water absorption, the shrinkage is quite high. The modified Eurocode shrinkage model, which had been calibrated by Kwan *et al.* [27] to account for the local conditions, was used. The variation of the concrete strength and secant modulus of elasticity with time were taken from the Structures Design Manual for Highways and Railways [28] of Hong Kong. Factors including the relative humidity and air temperature were based on the laboratory monitoring as well as those recorded by the Hong Kong Observatory.

Time-dependent analysis was carried out by either the time integration method (TIM) [29] or single-step method [30] adopting the age-adjusted elasticity modulus (AAEM) of concrete.

A prestressed concrete beam with a single corrugated steel web was fabricated for long-term monitoring as described in Section 2. The tendon force decreased with time as shown in Figure 12(a). The measured long-term loss of prestress was 10.4%. On the other hand, the upward long-term deflection at quarter points of span and middle span both increased as much as around 80%, as shown in Figures 12(b) and 12(c) respectively. The numerical results show reasonably good agreement with the experimental results.

To better understand the long-term behaviour of this type of bridges, the long-term behaviour of the prestressed concrete bridges with corrugated steel webs is compared with those of their counterparts with flat steel webs or concrete webs. A continuous bridge located in Shanghai, China was studied.

As shown in Figure 13(a), both the conventional bridges with flat steel webs and concrete webs have initial camber, which will reduce or even reverse due to time-dependent effects. In 100 years, it is predicted that the bridge with flat steel webs develops essentially downward deflections while that with concrete webs still retains some camber. Figure 13(a) shows that the bridge with corrugated steel webs has the largest change in deflection because of its high flexibility especially in shear, followed by the bridge with flat steel webs and then that with concrete webs.

Comparing the stresses at flange centroids as shown in Figure 13(b), the normal flange stresses in the bridge with flat steel webs have the highest reduction due to constraints of flat steel webs on the concrete creep and shrinkage. In the long term, the normal flange stresses of the bridge with corrugated steel webs approach those of the bridge with concrete webs. This can be attributed to that the effects of diaphragm and interaction between web shear deformation and local flange bending relieve with time.

As an alternative and simple approach, one may adopt the Eurocode approach to estimate the long-term deflection by using an effective modulus of elasticity for concrete with creep and accounting for shrinkage curvature. Parametric study on deflection, longitudinal displacement at beam end, prestressing force and normal stress of the bridge was also carried out by Chen *et al.* [31].

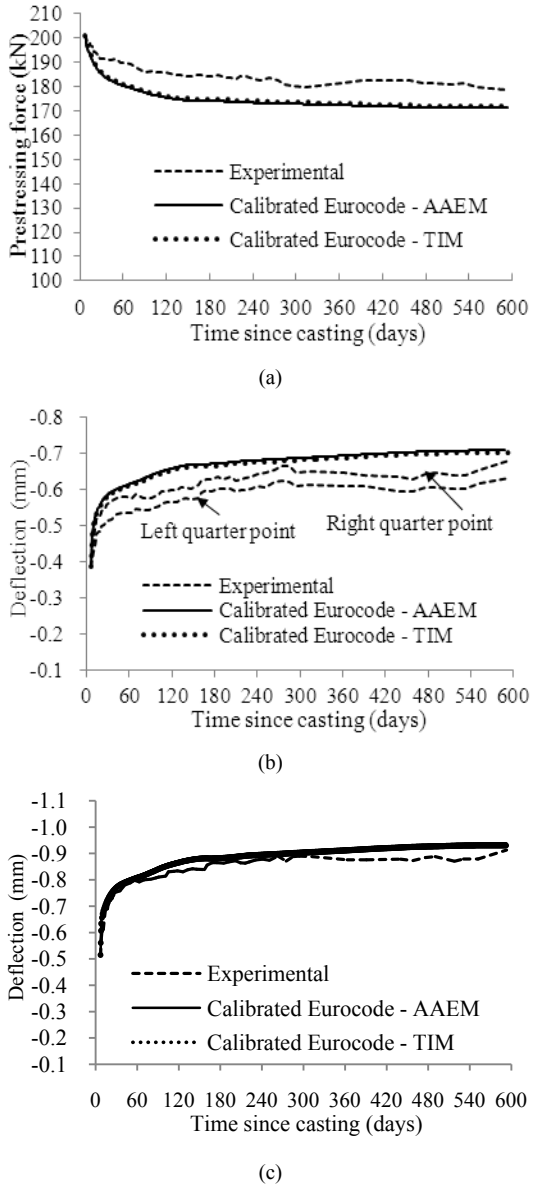

Figure 12. Long-term behaviour (a) Total prestressing force; (b) Quarter-point defection; and (c) Mid-span deflection

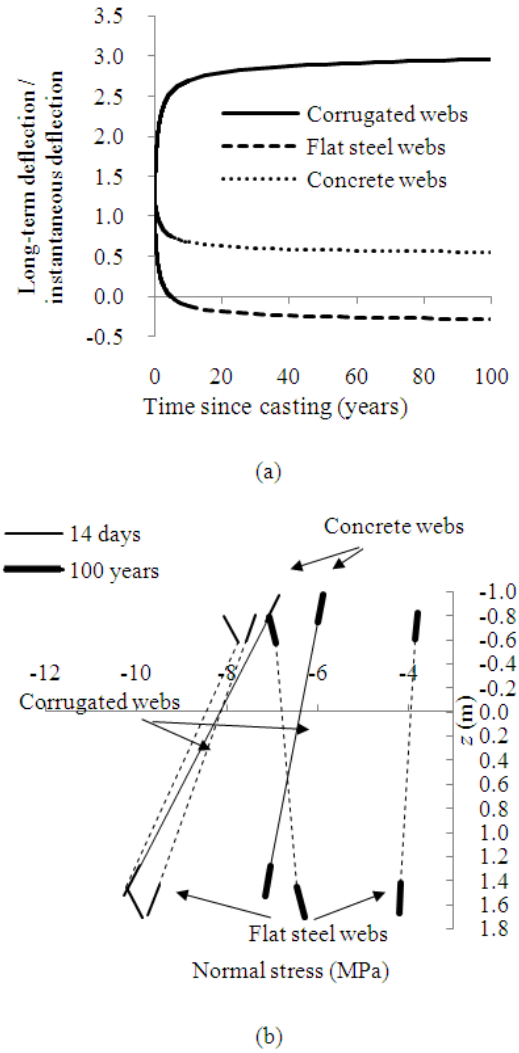

Figure 13. Numerical example: (a) Mid-span deflection with time; (b) Normal concrete stress distribution at middle span

8. Conclusions

In this study, the full-range and long-term structural behaviour of prestressed concrete bridges with corrugated steel webs has been investigated both numerically and experimentally. Based on the studies, the following conclusions can be drawn:

(a) Owing to the interaction between shear deformation of corrugated steel webs and local bending of concrete flanges, secondary bending moments and shear forces occur in the concrete flanges, which may violate of the common assumption of linear normal strain distribution over the entire section depth.

(b) The diaphragms of this type of bridges have minor effects on the deflections, but significant effects on stress distributions and stress resultants by constraining the web shear deformation in the vicinity and relative longitudinal movement of concrete flanges.

(c) For serviceability design, the shear and normal stress concentration in flanges due to the effects of diaphragm and interaction between web shear deformation and local bending of flanges should be examined carefully, especially in the vicinity of point loads and diaphragms. To relieve the stress concentration, diaphragms may be provided with haunches. At the ultimate limit state, there may be local failure of concrete flanges due to the stress concentration, especially in short bridges.

(d) With α as the square root of the ratio of equivalent shear rigidity of the beam section to the flange local flexural rigidity and L as the span length, the combined parameter αL is an indication of the effects of diaphragm and interaction between web shear deformation and flange local bending. The smaller the combined parameter αL is, the more significant these effects are.

(e) The diaphragms have significant effects on the natural frequencies and mode shapes only for bridges with short spans and/or lower ratios of the equivalent shear rigidity of beam section to flange local bending rigidity, namely for bridges with αL values below a certain limit.

(f) The effects of diaphragm and interaction between web shear deformation and local bending of flanges reduce gradually with time. The instantaneous deflections and long-term increment of this type of bridges are larger than those of their counterparts with concrete or flat steel webs, and therefore the deflections should be examined carefully. The long-term compressive normal stresses in the concrete flanges of this type of bridges are close to those of conventional bridges with concrete webs, but obviously larger than those of conventional bridges with flat steel webs.

(g) Concrete bridges with corrugated steel webs perform reasonably well in respect of sectional flexural ductility and deformability. In comparison with concrete box girder sections and solid concrete sections with comparable dimensions, concrete bridges with corrugated steel webs still perform well in respect of flexural ductility and deformability, provided that those with the same concrete sectional areas are compared. The effects of interaction between web shear deformation and local bending of concrete flanges on the sectional flexural ductility are sensitive to the arrangement of spans and loading, as well as sectional properties. The interaction effects decrease with increase of curvature. The interaction has little effect on the ultimate curvature and therefore deformability, but the interaction significantly increases the yield curvature and reduces the ductility.

(h) Owing to the presence of prestressing tendons and shear-deformable corrugated steel webs with negligible axial stiffness in this type of bridges, flange plastic hinge and full-depth plastic hinge may form and interact with each other. Experimental results show that the equivalent interactive plastic hinge length, critical region length and plastic behaviour are governed by the formation of flange plastic hinge. Based on the equivalent interactive plastic hinge length estimated by an empirical formula, a simplified method is proposed to predict the full-range structural behaviour of the bridge.

9. Design Recommendations

Some design recommendations for prestressed concrete bridges with corrugated steel webs are given below:

(a) To estimate the ultimate displacement and load, it is conservative to assume the plastic hinge to form only on one side of the critical section; otherwise the strength and ultimate displacement will be over-estimated. The arrangement of external tendons also affects the ductility, deformability and ultimate load of the bridge. Providing more intermediate deviators normally reduces the secondary effects and improves the ductility and deformability.

(b) The stress concentration due to effects of interaction between web shear deformation and local flange bending should be examined carefully, especially at the early stage.

(c) The use of a simple factor to predict the long-term deflection based on the instantaneous deflection could be misleading. A practical way is to use the effective modulus of elasticity of concrete with creep and the shrinkage curvature.

REFERENCES

[1] Cheyrezy, M. and Combault, J. (1990). Composite bridges with corrugated steel webs - achievements and prospects. IABSE Symposium on Mixed Structures including New Materials, Brussels: 479-484.

[2] Research Group of Composite Structure with Corrugated Steel Web (1998). Design Manual of PC Box Girders with Corrugated Steel Webs (in Japanese).

[3] Machimdamrong, C., Watanabe, E. and Ustunomiya, T. (2004). Analysis of corrugated steel web girders by an efficient beam bending theory. Structural Eng. / Earthquake Eng., JSCE, 21(2): 131s-142s.

[4] Briassoulis, D. (1986). Equivalent orthotropic properties of corrugated sheets. Comput. Struct., 23(2): 129-138.

[5] Elgaaly, M., Seshadri, A. and Hamilton, R.W. (1997). Bending strength of steel beams with corrugated webs. J. Struct. Eng., 123(6): 772-782.

[6] Combault, J. (1988). The Maupré Viaduct near Charolles, France. AISC National Steel Construction Conference, Miami Beach, Florida, USA: 1-12.

[7] Johnson, R.P. and Cafolla, J. (1997). Corrugated webs in plate girders for bridges, Proc. ICE Struct. Build., 122(2): 157-164.

[8] Chen X.C., Au F.T.K., Bai Z.Z. and Zeng Y. (2015b). An extended sandwich theory for prestressed concrete bridges with corrugated steel web(s). Report of IABSE Conference on "Elegance in Structures", Nara, 13-15 May. p. 270-271 and No. IA-22 in CD.

[9] Chen X.C., Li Z.H., Au F.T.K. and Jiang R.J. (2017a). Flexural vibration of prestressed concrete bridges with corrugated steel webs, International Journal of Structural Stability and Dynamics, 17(2), 1750023-1 to 1750023-30.

[10] Dall'Asta, A., Ragni, L. and Zona, A. (2007). Analytical model for geometric and material nonlinear analysis of externally prestressed beams. J. Eng. Mech., 133(1): 117-121.

[11] Ho, J.C.M., Kwan, A.K.H. and Pam H.J. (2003). Theoretical analysis of post-peak flexural behaviour of normal- and high-strength concrete beams. Struct. Des. Tall Spec., 12: 109-125.

[12] Bai, Z.Z. and Au, F.T.K. (2013). Flexural ductility design of high-strength concrete beams. Struct. Des. Tall Spec., 22: 521-542.

[13] Attard, M.M. and Setunge, S. (1996). The stress-strain relationship of confined and unconfined concrete. ACI Mater. J., 93(5), 432-442.

[14] Carreira, D.J. and Chu, K.H. (1986). The moment-curvature relationship of reinforced concrete members. ACI Struct. J., 83: 191-198.

[15] Guo, Z.H. and Zhang, X.Q. (1987). Investigation of complete stress-deformation curves for concrete in tension. ACI Mater. J., 84(4): 278-285.

[16] Mander, J.B., Priestley, M.J.N. and Park, R. (1984). Seismic design of bridge piers, Research report 84-2, Department of Civil Engineering, University of Canterbury, Christchurch.

[17] Menegotto, M. and Pinto, P.E. (1973). Method of analysis for cyclically loaded RC plane frames, including changes in geometry and non-elastic behaviour or elements under combined normal force and bending. IABSE preliminary report for symposium on resistance and ultimate deformability of structures acted on by well-defined repeated loads, Lisboa: 15-22.

[18] Chen X.C., Au F.T.K., Bai Z.Z., Li Z.H. and Jiang R.J. (2015a). Flexural ductility of reinforced and prestressed concrete sections with corrugated steel webs. Computers and Concrete, 16(4): 625-642.

[19] Pam, H.J. and Ho, J.C.M. (2009). Length of critical region for confinement steel in limited ductility high-strength reinforced concrete columns. Eng. Struct., 31: 2896-2908.

[20] Chen X.C., Zeng Y. and Au F.T.K. (2017c). Interaction of plastic hinges in prestressed concrete bridges with corrugated steel webs, Engineering Structures, 150: 359-372.

[21] Sheikh, S.A. and Khoury, S.S. (1993). Confined Concrete Columns with Stubs. ACI Struct. J., 90(4): 414-431.

[22] Bayrak, O. and Sheikh, S.A. (1997). High-strength concrete columns under simulated earthquake loading. ACI Strut. J., 94(6): 708-722.

[23] Subramanian, N. (2009). Discussion of "Plastic Hinge Length of Reinforced Concrete Columns" by Sungjin Bae and Oguzhan Bayrak. ACI struct. J., 106(2), Disc. 105-S28: 233-234.

[24] Baker, A.L.L. (1956). Ultimate load theory applied to the design of reinforced and prestressed concrete frames, Concrete Publications Ltd., London.

[25] Chen X.C., Bai Z.Z., Jiang R.J. and Au F.T.K. (2016). Prestressed concrete bridges with corrugated steel webs: Nonlinear analysis and experimental investigation, Steel and Composite Structures, 5(21), 1045-1067.

[26] Jiang, R.J., Au, F.T.K. and Xiao, Y. (2015). Prestressed concrete girder bridges with corrugated steel webs: Review. J. Struct. Eng., ASCE, 141(2), (04014108-1)-(04014108-9).

[27] Kwan, A.K.H, Au, F.T.K, Wong, H.H.C. and Ng, P.L. (2010). Shrinkage of Hong Kong granite aggregate concrete. Mag. Concrete Res., 62(2): 115-126.

[28] Highways Department of the Hong Kong Special Administrative Region (2013). Structures design manual for highways and Railways, The Government of the Hong Kong Special Administrative Region.

[29] Ghali, A., Favre, R. and Elbadry, M.M. (2002). Concrete Structures: Stresses and deformations (3rd edition), Spon Press, London.

[30] Bažant, Z.P. (1972). Prediction of concrete creep effects using age-adjusted effective modulus method. Journal of ACI, 69(4): 212-217.

[31] Chen X.C., Pandey M. and Au F.T.K. (2017b). Long-term behaviour of prestressed concrete bridges with corrugated steel webs, Journal of Bridge Engineering, 22(8), 04017040-1 to 04017040-9.